



## RESEARCH LETTER

10.1002/2017GL072855

## Key Points:

- Comprehensive climate models project a shorter duration of midlatitude precipitation extremes
- The duration is partly controlled by an advective time scale based on the mean zonal wind and the zonal length of events
- In an idealized climate model, increasing the meridional temperature gradient reduces the duration

## Supporting Information:

- Supporting Information S1

## Correspondence to:

J. G. Dwyer,  
jgdwyer@gmail.com

## Citation:

Dwyer, J. G., and P. A. O’Gorman (2017), Changing duration and spatial extent of midlatitude precipitation extremes across different climates, *Geophys. Res. Lett.*, 44, doi:10.1002/2017GL072855.

Received 28 JAN 2017

Accepted 29 MAY 2017

Accepted article online 12 JUN 2017

## Changing duration and spatial extent of midlatitude precipitation extremes across different climates

J. G. Dwyer<sup>1</sup>  and P. A. O’Gorman<sup>1</sup> 

<sup>1</sup>Department of Earth, Atmosphere and Planetary Sciences, Massachusetts Institute of Technology, Cambridge, Massachusetts, USA

**Abstract** Precipitation extremes intensify with climate warming in observations and simulations, but changes in their duration or spatial extent are not well understood. Here the duration and zonal length of midlatitude precipitation extremes are quantified in climate model simulations. Most comprehensive climate models project a decrease in duration over the 21st century, although the magnitude of the decrease with warming is less than 1% K<sup>-1</sup> in the multimodel mean. An advective time scale based on the mean zonal wind is shown to be linked to the duration in terms of spatial distribution, intermodel differences, and response to climate change. In simulations with an idealized climate model, a stronger meridional temperature gradient decreases the duration despite increases in the zonal length, and this is explained using the thermal wind relation and the Rossby deformation radius. However, the response of the zonal length to increasing mean temperature requires further study.

### 1. Introduction

Both observations and climate models show that the intensity of daily precipitation extremes increases with climate warming [e.g., O’Gorman, 2015]. But the typical duration of precipitation events is not fixed and can vary by season, region, and climate, and this can complicate interpretation of changes in daily precipitation extremes [e.g., Trenberth et al., 2003]. Some observational studies of present-day variability in precipitation extremes find sensitivities as large as 14% K<sup>-1</sup> with respect to surface temperature for hourly precipitation as compared to 7% K<sup>-1</sup> for daily precipitation [e.g., Lenderink and van Meijgaard, 2008; Westra et al., 2014]. Haerter et al. [2010] and Utsumi et al. [2011] found evidence that local warming can lead to a shorter duration of precipitation events, while Wasko and Sharma [2015] found that the temporal distribution of precipitation within storms became more peaked with increasing local temperature. These observational studies highlight the importance of a better understanding of the duration of precipitation extremes and how it might respond to climate change.

The effect of climate change on the temporal behavior of precipitation extremes has been examined previously both by defining contiguous precipitation events and by using a range of fixed accumulation periods. For simulations with global climate models (GCMs), Kao and Ganguly [2011] found that when intensity is plotted as a function of accumulation period on a log-log scale, to leading order the curves shift to larger intensities and keep their shape in response to climate warming, suggesting that changes in duration are small compared to changes in intensity. Similarly, using a convection-permitting model over the UK, Chan et al. [2016] found little change in the shape of the temporal profile of summertime extreme rainfall events under climate warming. However, using a convection-permitting model to simulate radiative-convective equilibrium over a wide range of temperatures, Singh and O’Gorman [2014] found that the sensitivity of precipitation extremes to warming varied with accumulation period for surface temperatures below 295 K, and this was at least partly attributed to the influence of ice and mixed-phase microphysics on the precipitation efficiency.

In this study we use GCM simulations to quantify the duration and zonal extent of extreme precipitation events, how they relate to the large-scale flow conditions, and how they respond to climate change. To reduce the dynamical importance of the parameterized convection in the GCMs, we focus on extratropical precipitation extremes and, in the case of comprehensive GCM simulations, extended winter seasons in which synoptic forcing is expected to be important for the precipitation extremes [e.g., Schumacher and Johnson, 2006].

Many physical factors can potentially affect the duration of precipitation extremes at a given location (e.g., cyclone and frontal dynamics, convective cell generation and motion, and microphysical processes), but one of the simplest and most universal factors is the advective influence of the large-scale mean flow. We quantify this influence using a simple advective time scale,

$$\tau = \frac{L}{U + U_0}, \quad (1)$$

where  $L$  is the zonal length of the precipitation event (i.e., the spatial extent of the event in the zonal direction),  $U$  is the absolute value of the time-averaged zonal wind at a nominal steering level for storms, and  $U_0 = 5 \text{ m s}^{-1}$ . We focus on the zonal direction for simplicity, and we exclude polar regions from our analysis to help ensure that zonal-mean advection is important. The offset  $U_0$  is included to represent meridional velocities, eddy zonal velocities, and internal storm dynamics; in practice, it prevents an unphysically long time scale in regions of weak mean zonal wind. For this advective time scale to be relevant to the duration of precipitation extremes, the storm lifetime must be greater than the advective time scale, and the spatial structure of the storm must not greatly change over the advective time scale. While this is clearly not true of all events, we will show that in the aggregate the duration of midlatitude precipitation extremes is linked to the advective time scale in both comprehensive and idealized GCM simulations and that the advective time scale is helpful for understanding the response of the duration to climate change.

The advective time scale is affected by both the zonal wind and the zonal length. Arctic amplification is weakening the low-level meridional temperature gradient [Screen and Simmonds, 2010], which would be expected to weaken the zonal winds by thermal wind balance. But the zonal winds are also affected by changes in meridional temperature gradients elsewhere and meridional shifts of the eddy-driven jets due to increasing greenhouse gases and ozone depletion or recovery [e.g., Polvani et al., 2011]. As a result, the projected response of the midlatitude zonal winds in the lower and middle troposphere involves regions of both increase and decrease [e.g., Grise and Polvani, 2014]. The zonal length may also change as the climate changes. Using station data from Australia, Wasko et al. [2016] found that precipitation becomes more concentrated toward the center of storms with local warming. Similarly, for idealized GCM simulations of climate warming, Shi and Durran [2016] found a more concentrated region of ascending motion in extratropical cyclones, while Pfahl et al. [2015] found that the region of heavy precipitation within intense extratropical cyclones became more tightly centered. The spatial extent of precipitation may be partly controlled by the overall size of midlatitude eddies (the eddy length), and Kidston et al. [2010] found that the eddy length robustly increased with warming in comprehensive GCMs.

We first describe our method to identify extreme precipitation events and to calculate their duration and zonal length (section 2). We then present results for the duration and zonal length in comprehensive GCMs and an observational data set, and we demonstrate the relevance of the advective time scale for duration in terms of spatial distribution, intermodel differences, and the response to climate change (section 3). We next use the advective time scale to explain why the duration decreases with increasing meridional temperature gradient in idealized GCM simulations with different meridional insolation gradients (section 4). Finally, we summarize our results and discuss their implications (section 5).

## 2. Characterization of Duration and Extent of Precipitation Extremes

We use high percentiles of precipitation intensity (i.e., hourly or 3-hourly precipitation) to identify extreme events and their start and end times, as described in detail below. This approach allows comparison with the many previous studies that have identified precipitation extremes in terms of precipitation intensity. Unlike previous studies of precipitation events, we choose not to use a fixed intensity threshold to define the start and end times of the events because a low fixed threshold (e.g.,  $0.1 \text{ mm h}^{-1}$ ) would be subject to the drizzle problem in the GCMs, and the use of any fixed threshold may give a tendency for durations to increase with warming simply because precipitation intensities increase with warming.

We first identify the times when the precipitation rate exceeds a threshold  $I$  defined as a high percentile of the precipitation rate. The threshold is calculated separately for each climate analyzed, and at each grid box for the comprehensive GCMs or at each latitude for the idealized GCM which is statistically zonally symmetric. The percentiles are calculated over all time, including when it is not precipitating. The precipitation rate used is over the shortest accumulation period available: 3-hourly for output from the comprehensive GCMs and hourly for output from the idealized GCM. (Results were very similar for the idealized GCM when the analysis

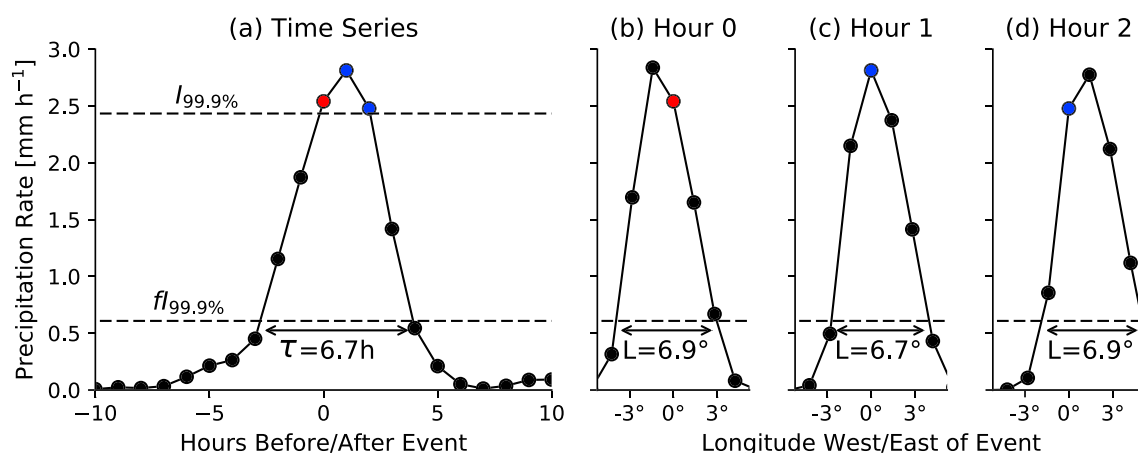


**Figure 1.** An example of the (a) duration and (b–d) zonal length identification of a single extreme precipitation event from the idealized GCM. Shown are three exceedances of the 99.9th percentile of hourly precipitation at a particular latitude,  $I_{99.9\%} = 2.4 \text{ mm h}^{-1}$ . The second and third exceedances (blue markers) follow consecutively from the first (red marker), and all three are combined into one event. The duration of this event is the length of time that precipitation is greater than 25% of  $I_{99.9\%}$ . The zonal length is similarly defined as the zonal distance over which precipitation is greater than 25% of  $I_{99.9\%}$ , and it is calculated for each of the three exceedances and then averaged to provide a single length scale for the event.

was repeated using 3-hourly averaged precipitation rates). Next we combine consecutive exceedances into events to make them more independent. An example of this procedure is shown in the time series in Figure 1a in which the first exceedance in red is combined with the following two exceedances in blue. The duration of the event is defined as the time over which the precipitation rate is higher than a fraction  $f$  of the threshold intensity. The start and end of each event are determined by linear interpolation around the times when the precipitation rate crosses the fractional threshold. We choose  $f < 1$  because precipitation before and after a period of high-intensity precipitation is important for impacts and because typical durations would be near the sampling frequency if  $f = 1$  were used. Additionally, we choose  $f > 0$  since GCMs overestimate the frequency of precipitation compared to observations by simulating too much drizzle [Stephens *et al.*, 2010]. We present results for the threshold  $I$  at the 99.9th percentile and for  $f = 0.25$ . Using a less extreme intensity threshold (like the 99th percentile for  $I$ ) yields more events and smoother results that are similar to the 99.9th percentile case except for the response to climate change in extended summer seasons as described in Text S1 in the supporting information. Choosing a larger threshold fraction (such as  $f = 0.5$ ) also does not change our conclusions.

The zonal length  $L$  is determined in a similar manner. For each exceedance, we determine the distance west and east of the event's longitude where the precipitation is larger than  $fI$ , as depicted in Figure 1b. If there is more than one exceedance in an event, we average the zonal length for all exceedances (Figures 1b–1d) to determine the length scale of the event.

### 3. Comprehensive Climate Models and Observations

We begin by analyzing extended winter seasons in simulations from a set of 10 comprehensive atmosphere-ocean climate models included in phase 5 of the Coupled Model Intercomparison Project (CMIP5) [Taylor *et al.*, 2012]. We only include models for which 3-hourly precipitation rates were available (listed in the caption of Figure 3). The extended winter seasons used are November–March (NDJFM) in the Northern Hemisphere (NH) and May–September (MJJAS) in the Southern Hemisphere (SH). We analyze the historical simulations over 1980–1999 as the control climate, and the RCP8.5 simulations over 2080–2099 as a future warmer climate. For each GCM, climate and grid box, we identify the extreme events (there are 17.2 on average in the historical simulations) and calculate their median duration and zonal length.

There are substantial spatial variations in the duration of midlatitude precipitation extremes as shown in Figure 2a for the extended winter seasons. These include a land-ocean contrast, with longer durations over land. The zonal-mean duration minimizes roughly at  $50^\circ\text{N}$  and  $50^\circ\text{S}$  and increases equatorward and poleward from there. While there are some differences between individual models (not shown), all of them have similar spatial structures with longer durations over land and minimums in latitude at roughly  $45^\circ$ – $50^\circ$  in each hemisphere.

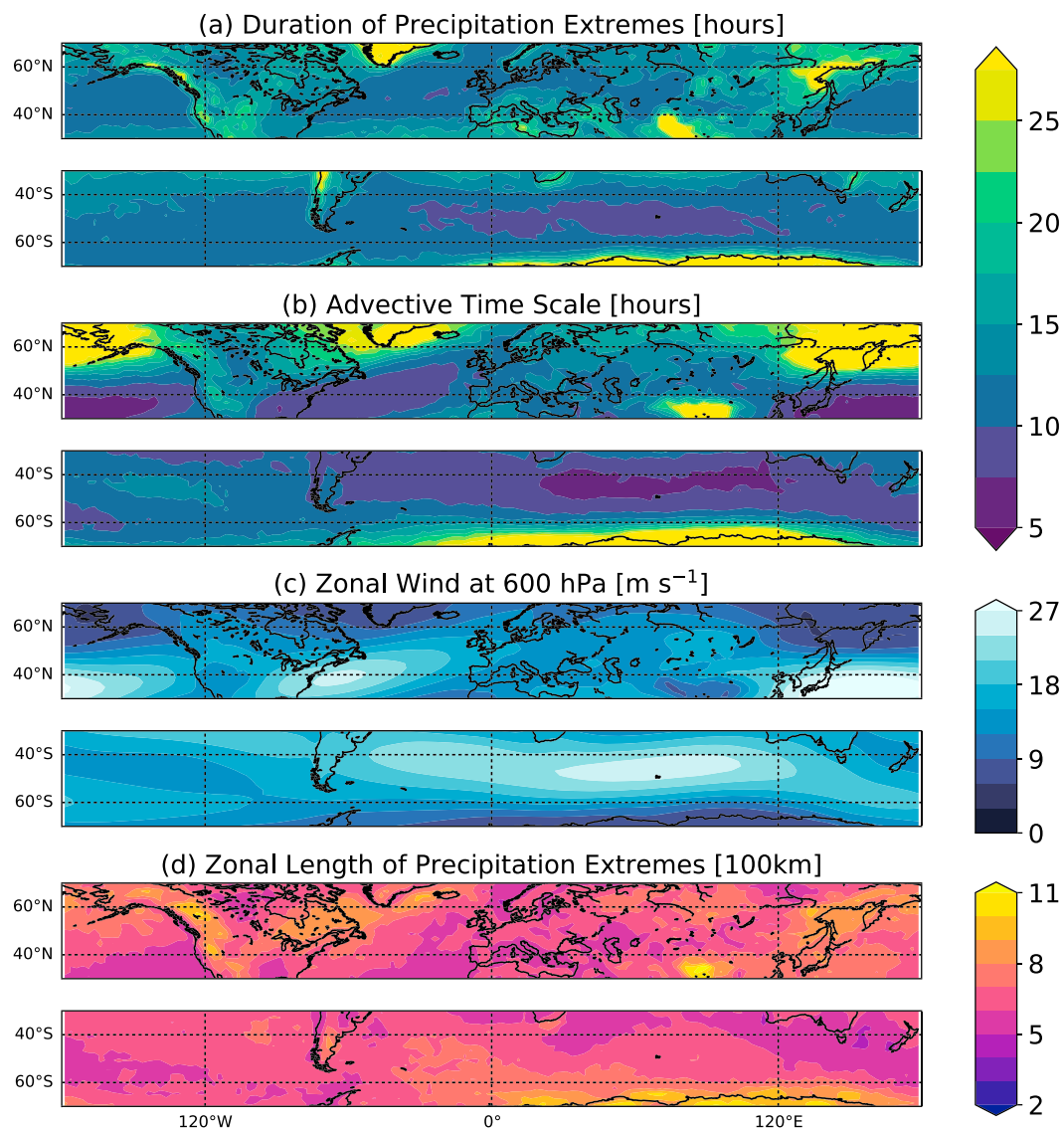


**Figure 2.** The 1980–1999 CMIP5 multimodel mean (a) duration of precipitation extremes in hours, (b) advective time scale in hours, (c) absolute value of the time-mean zonal wind at 600 hPa in  $\text{m s}^{-1}$ , and (d) zonal length of precipitation extremes in units of 100 km for extended winter seasons (NDJFM in the NH and MJJAS in the SH).

The advective time scale, calculated with the zonal length of events, the absolute value of the time-mean zonal wind at 600 hPa, and  $U_0 = 5 \text{ m s}^{-1}$ , is shown in Figure 2b. The advective time scale has a similar spatial structure to the duration, although it is somewhat shorter than the duration equatorward of  $50^\circ$  and longer at higher latitudes. The specific choices of  $U_0$  and the pressure level for the zonal wind are physically reasonable and give a good overall match of the advective time scale to the duration; different choices would affect the magnitude of the advective time scale, but have a smaller effect on the spatial pattern.

The advective time scale has many spatial features in common with the zonal wind shown in Figure 2c. In particular, zonal wind maxima correspond to advective time scale minima. The zonal length of precipitation extremes in Figure 2d does not exhibit a clear land-ocean contrast and has as much longitudinal variability as latitudinal variability.

Figure 3a shows that the duration averaged over  $30^\circ - 70^\circ$  correlates well across models with the spatially averaged advective time scale, with a correlation coefficient of  $r = 0.85$ . However, the slope of the least squares regression line is considerably smaller than one, which indicates that processes other than zonal advection are also important for the duration and that these other processes are not fully represented by the constant

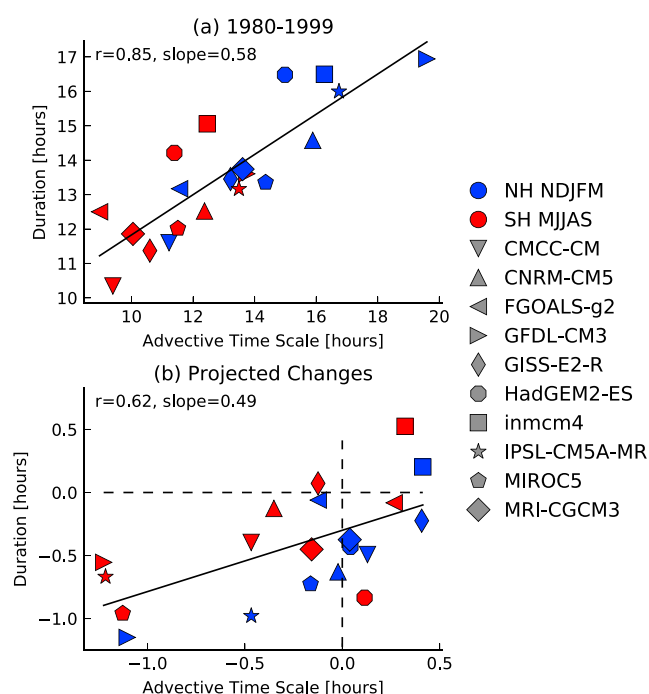


**Figure 3.** Scatterplot of the duration of precipitation extremes and the advective time scale averaged between 30° and 70° latitude in each hemisphere’s extended winter season for different CMIP5 models (a) over 1980–1999 in the historical simulations and (b) the difference in each quantity between 2080–2099 in the RCP8.5 simulations and 1980–1999 in the historical simulations. NH extended winter is in blue, SH extended winter is in red, and different CMIP5 models are indicated with different marker shapes. Solid lines are the least squares regression relationships. Correlation coefficients and regression slopes are given in each panel. Units are hours. Dashed lines in Figure 3b indicate zero values.

scale and duration are correlated ( $r = 0.62$ ), although changes in duration are smaller than changes in advective time scale with a least squares regression slope of 0.49.

Figure S5 shows the latitudinal structure of the zonal-mean fractional changes and reveals that multimodel mean changes in duration are relatively small between 30°–45° in the southern hemisphere and that there is not a detailed correspondence between the changes in duration and advective time scale. Increases in zonal wind drive decreases in advective time scale to a greater extent than do zonal length changes; the fractional changes in zonal length are small except southward of 50°S.

Results for extended summer seasons are described in Text S1 and are similar to the extended winter case in most regards (e.g., there is a multimodel reduction in duration of  $0.7\% K^{-1}$  as compared to a  $6.1\% K^{-1}$  increase in intensity), but the results from the CMIP5 models are expected to be less reliable in summer because of the greater role of convection. Satellite-based estimates of precipitation are complementary to the models in that they are considered more reliable in summer than in winter in midlatitudes [Ebert *et al.*, 2007; Guo *et al.*, 2015], at least over land. Therefore, in Text S2 we describe an observational analysis of the duration and zonal length for extended summer seasons based on CMORPH satellite precipitation data [Joyce *et al.*, 2004] and comparison to the advective time scale using ERA-Interim reanalysis for zonal winds [Dee *et al.*, 2011]. The observed duration is shorter than the multimodel mean of the CMIP5 models, but it has a similar magnitude and spatial distribution as the observed advective time scale (Figures S6 and S7).

Overall, our results suggest that the duration is linked to the advective time scale for both the present climate and the response to climate change. Most of the CMIP5 models project a reduction in duration, although the reduction in duration is small compared with the increase in intensity.

offset  $U_0$ . Changing the steering level or  $U_0$  used to calculate the advective time scale does not greatly change the correlation coefficient but does alter the slope (a larger value of  $U_0$  gives a slope closer to one but does not greatly change the y intercept). For a lower intensity threshold of the 99th percentile, the correlation coefficient is higher at  $r = 0.96$  and the slope is also higher (Figure S4a).

Compared to 1980–1999, most of the CMIP5 models project a shorter duration of midlatitude precipitation extremes for 2080–2099 under the RCP8.5 scenario (Figure 3b) with changes ranging from roughly a 1 h decrease to a 30 min increase. The multimodel mean fractional decrease of the spatially averaged duration is 0.03, which corresponds to a reduction of  $0.7\% K^{-1}$  when normalized by the change in the annual, global-mean surface air temperature of each model. This is considerably smaller than the  $5.8\% K^{-1}$  increase in the spatially averaged intensity, where intensity is measured by the 99.9th percentile of 3-hourly precipitation at each grid box. Figure 3b shows that the advective time scale also decreases for most models and that the changes in advective time

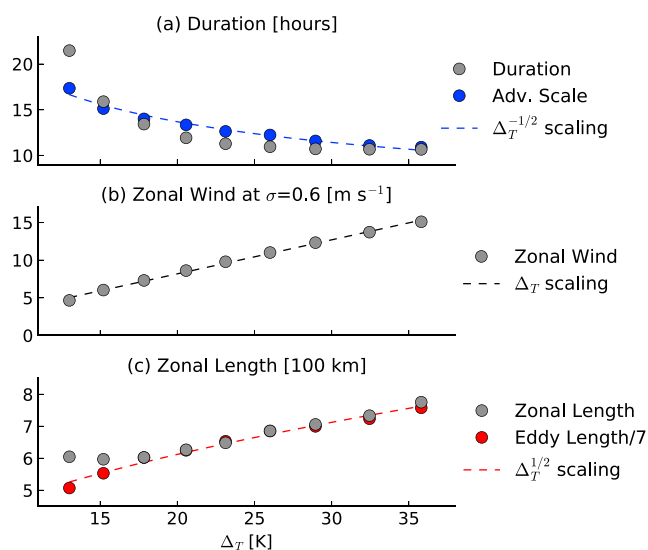


**Figure 4.** Results from the idealized GCM as a function of meridional temperature difference  $\Delta_T$ . Each marker represents the value averaged over  $30^\circ - 70^\circ$  in both hemispheres. (a) Duration of precipitation extremes (gray markers) and advective time scale (blue markers) in hours and a scaling  $\Delta_T^{-1/2}$  fit to the advective time scale (dashed blue). (b) Mean zonal wind at  $\sigma=0.6$  (gray markers) in  $\text{m s}^{-1}$  and a scaling  $\Delta_T$  fit to the zonal wind (dashed black). (c) Zonal length of precipitation extremes (gray markers) and eddy length divided by a factor of 7 (red markers) in units of 100 km and a scaling  $\Delta_T^{1/2}$  fit to the eddy length (dashed red).

spectral resolution and a different range of  $\Delta_s$ . We analyze 1000 days after a 1000 day spin-up from an isothermal state for each simulation. Precipitation rates are stored hourly. Results are averaged across longitudes and hemispheres to take advantage of the statistical symmetries of the model. Since the primary changes in climate relate to the changes in meridional temperature gradient rather than in global-mean temperature, we present our results as a function of the meridional temperature difference,  $\Delta_T$ , across the midlatitude band  $30^\circ - 70^\circ$  as calculated using a linear least squares fit of surface air temperature to latitude across this band.

Figure 4a shows that the duration averaged over the midlatitudes decreases as  $\Delta_T$  increases. The sensitivity of duration to  $\Delta_T$  is largest for climates with  $\Delta_T < 25$  K. The advective time scale, calculated from the mean zonal wind at  $\sigma = 0.6$  with  $U_0 = 5 \text{ m s}^{-1}$ , also decreases with increasing  $\Delta_T$  and agrees reasonably well with the duration although it is somewhat larger in value for most of the simulations (Figure 4a).

The advective time scale depends on the zonal wind and the zonal length of precipitation extremes. The zonal wind increases linearly with increasing  $\Delta_T$  as expected from the thermal wind relation (Figure 4b). The zonal length also increases with  $\Delta_T$  over most of the climates, although it stays roughly constant for  $\Delta_T < 20$  K (Figure 4c). To understand the changes in zonal length, we also calculate the eddy length at each latitude following *Kidston et al.* [2010], using the eddy kinetic energy spectrum based on the high-pass-filtered meridional wind at  $\sigma = 0.6$ . The eddy length calculated in this way is about a factor of 7 larger than the zonal length of precipitation extremes, but it increases with increasing  $\Delta_T$  at a similar fractional rate, except for simulations with  $\Delta_T < 20$  K. Thus, the increase in zonal length of precipitation extremes with  $\Delta_T$  seems to be simply related to an increase in the size of the eddies in which the precipitation is embedded.

There is also some spatial structure to the changes in duration and zonal length across the midlatitudes as shown in Figure S8. The decreases in duration with increasing  $\Delta_T$  are largest at lower latitudes, and this behavior is captured by the advective time scale. While there are large increases in zonal wind at all latitudes, the zonal length does not increase at lower latitudes, and hence, the advective time scale decreases to a greater extent at lower latitudes.

The increases in zonal wind and zonal length with increasing  $\Delta_T$  have opposing effects on the advective time scale. Why do the increases in zonal wind win out, causing the advective time scale to decrease? To answer this

#### 4. Varying Meridional Temperature Gradient in an Idealized GCM

To further investigate the links between the advective time scale and the duration of precipitation extremes, we next analyze simulations with an idealized GCM in which there are large changes in the meridional temperature gradient and thus in the zonal winds. The idealized GCM follows *Frierson et al.* [2006] and *Frierson* [2007] with details as in *O’Gorman and Schneider* [2008a]. The lower boundary condition is a zonally symmetric and static mixed layer ocean, longwave radiation is represented using a two-stream gray radiation scheme, and there are no diurnal or seasonal cycles. The spectral resolution is T85 and there are 30 vertical  $\sigma$  levels. We analyze a series of nine simulations in which the insolation gradient parameter,  $\Delta_s$ , is varied from 0.2 to 1.8 in increments of 0.2. These simulations are similar to those described in *O’Gorman and Schneider* [2008b], except that here we use a higher

question, we need to know how the eddy length scales with  $\Delta_T$  since this gives the scaling of the zonal length of precipitation extremes. The eddy length has previously been found to scale with the Rossby deformation radius [Merlis and Schneider, 2009; Kidston et al., 2010; O’Gorman, 2011]. Neglecting changes in the latitude of the storm track and depth of the troposphere, the Rossby deformation radius is expected to scale with the buoyancy frequency which may be calculated using the effective static stability of O’Gorman [2011] to account for latent heating. Further, assuming that the supercriticality is approximately constant as found in previous simulations [Schneider and Walker, 2006; O’Gorman, 2011], the buoyancy frequency is expected to scale with the square root of the meridional temperature gradient,  $\Delta_T^{1/2}$ . Thus, we expect the eddy length to scale with  $\Delta_T^{1/2}$ , and this is the case in the simulations as shown in Figure 4c. Then given that  $\tau \sim LU^{-1}$ ,  $L \sim \Delta_T^{1/2}$ , and  $U \sim \Delta_T$  based on thermal wind, we expect that  $\tau \sim \Delta_T^{-1/2}$ , and this scaling captures the behavior of the advective time scale as shown in Figure 4a. Importantly, this argument explains why the advective time scale should be expected to decrease with increasing  $\Delta_T$  despite increases in the zonal length of the precipitation extremes.

Kidston et al. [2011] argued that eddies increase their intrinsic westward phase speed relative to the zonal wind as the eddy length increases, and this could partially counterbalance the increasing mean westerly winds with increasing  $\Delta_T$ . However, Text S3 shows that the advective time scale still maintains the  $\Delta_T^{-1/2}$  scaling when it is calculated using the eddy phase speed [cf. Randel and Held, 1991] rather than the mean zonal wind.

Overall, we find that the duration decreases for increasing  $\Delta_T$  as a result of faster zonal winds, offset to some extent by increases in zonal length, and that the increases in zonal length result from increases in the size of the eddies in which the precipitation is embedded. Consistent with our interpretation, Graff and LaCasce [2014] found faster eastward cyclone translation speeds with increasing meridional temperature gradient in an atmospheric GCM, and they also found faster poleward translation speeds and decreases in cyclone lifetime which could contribute to decreases in precipitation duration.

## 5. Conclusions

In this study, we have defined event-based measures for the duration and zonal length of precipitation extremes. Such measures are important because both the duration and spatial extent of extreme events influence their societal impacts. Most of the CMIP5 models project an overall reduction in the duration of mid-latitude precipitation extremes over the 21st century. However, this reduction is small compared to increases in the intensity of precipitation extremes ( $0.7\% \text{ K}^{-1}$  as compared to  $5.8\% \text{ K}^{-1}$  for the extended winter seasons). Conceptualizing the storms as being embedded in the large-scale flow, we introduce a simple advective time scale and find that it is linked to the duration of precipitation extremes in terms of spatial distribution, inter-model differences, and the response to climate change. According to the advective time scale, the shorter duration projected by the CMIP5 models is mainly driven by stronger westerlies. That is, stronger winds are advecting the storms faster, shortening the length of time that any surface location experiences extreme precipitation, though changes in the zonal length of the storms also affect the advective time scale.

Our CMIP5 results are considered most reliable for large-scale, primarily nonconvective events in the extended winter seasons. For the extended summer seasons, we have also used satellite-derived precipitation data to show that there are some similar spatial variations in the duration and advective time scale. Future modeling studies could further investigate the summertime relationship of the duration and advective time scale using higher-resolution models (as compared to CMIP5) that better represent extreme convective precipitation.

We also analyzed the responses of duration and zonal length to changes in meridional temperature gradient using an idealized GCM. Duration was found to decrease with increasing meridional temperature gradient due to increases in zonal wind that outpace increases in zonal length. The greater relative effect of the changes in zonal wind was explained using thermal wind balance and the scaling of the zonal length with the eddy length and thus the Rossby deformation radius.

The changes in zonal length in the idealized GCM simulations were found to be related to changes in the size of eddies in which the precipitation events were embedded. However, we find that this link between zonal extent of precipitation extremes and eddy length does not hold for the idealized GCM when the longwave optical depth is varied rather than the meridional insolation gradient (not shown). Similarly for the comprehensive climate model projections, we find changes in zonal length of both signs depending on latitude in the CMIP5 models, but previous work has found robust increases in eddy length with warming [Kidston et al., 2010].

These results suggest that warming and moistening of the atmosphere may affect the spatial extent of the precipitation in addition to any influence from changes in the overall size of eddies [cf. *Shi and Durran*, 2016; *Pfahl et al.*, 2015; *Wasko et al.*, 2016]; this effect may be related to increases in the magnitude of the skewness of the vertical velocity with warming [*Pendergrass and Gerber*, 2016].

Overall, we find that the advective time scale provides a useful link between the duration of precipitation extremes and the mean state of the atmosphere. Other physical factors also affect the duration of precipitation extremes, and their contribution to the climate change response requires further study. We have given an explanation for changes in spatial extent in response to changes in meridional temperature gradient, but it is also important to understand the response of spatial extent to an overall warming and moistening of the atmosphere. It would also be of interest to investigate whether similar changes in spatial extent and duration are obtained using alternative definitions of extreme precipitation events, such as extremes based on event accumulation rather than intensity [cf. *Neelin et al.*, 2017].

### Acknowledgments

J.G.D. is supported by an NSF AGS Postdoctoral Research Fellowship under award 1433290. P.A.O.G. acknowledges support from NSF AGS 1552195. We thank two reviewers for their helpful comments. We acknowledge the World Climate Research Programme's Working Group on Coupled Modelling, which is responsible for CMIP, and we thank the climate modeling groups for producing and making available their model output. CMIP5 model output is available from the Earth System Grid, and the idealized GCM model output is available from the authors upon request. CMORPH-CRT precipitation data were provided by NOAA CPC at [ftp://ftp.cpc.ncep.noaa.gov/precip/CMORPH\\_V1.0/CRT/0.25deg-3HLY/](ftp://ftp.cpc.ncep.noaa.gov/precip/CMORPH_V1.0/CRT/0.25deg-3HLY/). The ERA-Interim reanalysis was produced and provided by the European Centre for Medium-Range Weather Forecasts. Processed duration and zonal length data are available at <http://hdl.handle.net/1721.1/109727>.

### References

- Chan, S. C., E. J. Kendon, N. M. Roberts, H. J. Fowler, and S. Blenkinsop (2016), The characteristics of summer sub-hourly rainfall over the southern UK in a high-resolution convective permitting model, *Environ. Res. Lett.*, *11*, 094024, doi:10.1088/1748-9326/11/9/094024.
- Dee, D. P., et al. (2011), The ERA-Interim reanalysis: Configuration and performance of the data assimilation system, *Q. J. R. Meteorol. Soc.*, *137*, 553–597, doi:10.1002/qj.828.
- Ebert, E. E., J. E. Janowiak, and C. Kidd (2007), Comparison of near-real-time precipitation estimates from satellite observations and numerical models, *Bull. Am. Meteorol. Soc.*, *88*, 47–64, doi:10.1175/BAMS-88-1-47.
- Frierson, D. M. W. (2007), The dynamics of idealized convection schemes and their effect on the zonally averaged tropical circulation, *J. Atmos. Sci.*, *64*, 1959–1976, doi:10.1175/JAS3935.1.
- Frierson, D. M. W., I. M. Held, and P. Zurita-Gotor (2006), A gray-radiation aquaplanet moist GCM. Part I: Static stability and eddy scale, *J. Atmos. Sci.*, *63*, 2548–2566, doi:10.1175/JAS3753.1.
- Graff, L. S., and J. H. LaCasce (2014), Changes in cyclone characteristics in response to modified SSTs, *J. Clim.*, *27*, 4273–4295, doi:10.1175/JCLI-D-13-00353.1.
- Grise, K. M., and L. M. Polvani (2014), The response of midlatitude jets to increased CO<sub>2</sub>: Distinguishing the roles of sea surface temperature and direct radiative forcing, *Geophys. Res. Lett.*, *41*, 6863–6871, doi:10.1002/2014GL061638.
- Guo, H., S. Chen, A. Bao, J. Hu, A. S. Gebregiorgis, X. Xue, and X. Zhang (2015), Inter-comparison of high-resolution satellite precipitation products over Central Asia, *Remote Sens.*, *7*, 7181–7211, doi:10.3390/rs70607181.
- Haerter, J. O., P. Berg, and S. Hagemann (2010), Heavy rain intensity distributions on varying time scales and at different temperatures, *J. Geophys. Res.*, *115*, D17102, doi:10.1029/2009JD013384.
- Joyce, R. J., J. E. Janowiak, P. A. Arkin, and P. Xie (2004), CMORPH: A method that produces global precipitation estimates from passive microwave and infrared data at high spatial and temporal resolution, *J. Hydrometeorol.*, *5*, 487–503, doi:10.1175/1525-7541(2004)005<0487:CAMTPG>2.0.CO;2.
- Kao, S.-C., and A. R. Ganguly (2011), Intensity, duration, and frequency of precipitation extremes under 21st-century warming scenarios, *J. Geophys. Res.*, *116*, D16119, doi:10.1029/2010JD015529.
- Kidston, J., S. M. Dean, J. A. Renwick, and G. K. Vallis (2010), A robust increase in the eddy length scale in the simulation of future climates, *Geophys. Res. Lett.*, *37*, L03806, doi:10.1029/2009GL041615.
- Kidston, J., G. K. Vallis, S. M. Dean, and J. A. Renwick (2011), Can the increase in the eddy length scale under global warming cause the poleward shift of the jet streams?, *J. Clim.*, *24*, 3764–3780, doi:10.1175/2010JCLI3738.1.
- Lenderink, G., and E. van Meijgaard (2008), Increase in hourly precipitation extremes beyond expectations from temperature changes, *Nat. Geosci.*, *1*, 511–514, doi:10.1038/ngeo262.
- Merlis, T. M., and T. Schneider (2009), Scales of linear baroclinic instability and macroturbulence in dry atmospheres, *J. Atmos. Sci.*, *66*, 1821–1833, doi:10.1175/2008JAS2884.1.
- Neelin, J. D., S. Sahany, S. N. Stechmann, and D. N. Bernstein (2017), Global warming precipitation accumulation increases above the current-climate cutoff scale, *Proc. Natl. Acad. Sci.*, *114*, 1258–1263, doi:10.1073/pnas.1615333114.
- O'Gorman, P. A. (2011), The effective static stability experienced by eddies in a moist atmosphere, *J. Atmos. Sci.*, *68*, 75–90, doi:10.1175/2010JAS3537.1.
- O'Gorman, P. A. (2015), Precipitation extremes under climate change, *Curr. Clim. Change Rep.*, *1*, 49–59, doi:10.1007/s40641-015-0009-3.
- O'Gorman, P. A., and T. Schneider (2008a), The hydrological cycle over a wide range of climates simulated with an idealized GCM, *J. Clim.*, *21*, 3815–3832, doi:10.1175/2007JCLI2065.1.
- O'Gorman, P. A., and T. Schneider (2008b), Energy of midlatitude transient eddies in idealized simulations of changed climates, *J. Clim.*, *21*, 5797–5806, doi:10.1175/2008JCLI2099.1.
- Pendergrass, A. G., and E. P. Gerber (2016), The rain is askew: Two idealized models relating the vertical velocity and precipitation distributions in a warming world, *J. Clim.*, *29*, 6445–6462, doi:10.1175/JCLI-D-16-0097.1.
- Pfahl, S., P. A. O'Gorman, and M. S. Singh (2015), Extratropical cyclones in idealized simulations of changed climates, *J. Clim.*, *28*, 9373–9392, doi:10.1175/JCLI-D-14-00816.1.
- Polvani, L. M., D. W. Waugh, G. J. P. Correa, and S.-W. Son (2011), Stratospheric ozone depletion: The main driver of twentieth-century atmospheric circulation changes in the Southern Hemisphere, *J. Clim.*, *24*, 795–812, doi:10.1175/2010JCLI3772.1.
- Randel, W. J., and I. M. Held (1991), Phase speed spectra of transient eddy fluxes and critical layer absorption, *J. Atmos. Sci.*, *48*, 688–697, doi:10.1175/1520-0469(1991)048<0688:PSSOTE>2.0.CO;2.
- Schneider, T., and C. C. Walker (2006), Self-organization of atmospheric macroturbulence into critical states of weak nonlinear eddy–eddy interactions, *J. Atmos. Sci.*, *63*, 1569–1586, doi:10.1175/JAS3699.1.
- Schumacher, R. S., and R. H. Johnson (2006), Characteristics of US extreme rain events during 1999–2003, *Weather Forecasting*, *21*, 69–85, doi:10.1175/WAF900.1.
- Screen, J., and I. Simmonds (2010), The central role of diminishing sea ice in recent Arctic temperature amplification, *Nature*, *464*, 1334–1337, doi:10.1038/nature09051.

- Shi, X., and D. Durran (2016), Sensitivities of extreme precipitation to global warming are lower over mountains than over oceans and plains, *J. Clim.*, *29*, 4779–4791, doi:10.1175/JCLI-D-15-0576.1.
- Singh, M. S., and P. A. O’Gorman (2014), Influence of microphysics on the scaling of precipitation extremes with temperature, *Geophys. Res. Lett.*, *41*, 6037–6044, doi:10.1002/2014GL061222.
- Stephens, G. L., T. L’Ecuyer, R. Forbes, A. Gettleman, J.-C. Golaz, A. Bodas-Salcedo, K. Suzuki, P. Gabriel, and J. Haynes (2010), Dreary state of precipitation in global models, *J. Geophys. Res.*, *115*, D24211, doi:10.1029/2010JD014532.
- Taylor, K. E., R. J. Stouffer, and G. A. Meehl (2012), An overview of CMIP5 and the experiment design, *Bull. Am. Meteorol. Soc.*, *93*, 485–498, doi:10.1175/BAMS-D-11-00094.1.
- Trenberth, K. E., A. Dai, R. M. Rasmussen, and D. B. Parsons (2003), The changing character of precipitation, *Bull. Am. Meteorol. Soc.*, *84*, 1205–1217, doi:10.1175/BAMS-84-9-1205.
- Utsumi, N., S. Seto, S. Kanae, E. E. Maeda, and T. Oki (2011), Does higher surface temperature intensify extreme precipitation?, *Geophys. Res. Lett.*, *38*, L16708, doi:10.1029/2011GL048426.
- Wasko, C., and A. Sharma (2015), Steeper temporal distribution of rain intensity at higher temperatures within Australian storms, *Nat. Geosci.*, *8*, 527–529, doi:10.1038/ngeo2456.
- Wasko, C., A. Sharma, and S. Westra (2016), Reduced spatial extent of extreme storms at higher temperatures, *Geophys. Res. Lett.*, *43*, 4026–4032, doi:10.1002/2016GL068509.
- Westra, S., H. J. Fowler, J. P. Evans, L. V. Alexander, P. Berg, F. Johnson, E. J. Kendon, G. Lenderink, and N. M. Roberts (2014), Future changes to the intensity and frequency of short-duration extreme rainfall, *Rev. Geophys.*, *52*, 522–555, doi:10.1002/2014RG000464.